

Buckling and collapse analysis of a cracked panel under a sequence of tensile to compressive load employing a shell-solid mixed finite element modeling

Satoyuki Tanaka^{a,*}, Septia Hardy Sujiatanti^{a,b}, Yu Setoyama^{a,c},
Ji Yu^d, Daisuke Yanagihara^e, Zhiyong Pei^f

^a*Graduate School of Engineering, Hiroshima University, Japan,
e-mail: satoyuki@hiroshima-u.ac.jp*

^b*Department of Naval Architecture, Institut Teknologi Sepuluh Nopember, Indonesia,
e-mail: septia.rahmadiano@gmail.com*

^c*Fujitsu Kyushu Systems Limited, Japan, e-mail: ysetoyama@jp.fujitsu.com*

^d*Wuhan Institute of Shipbuilding Technology, PR China, e-mail: tc2462@163.com*

^e*Faculty of Engineering, Kyushu University, Japan,
e-mail: yanagihara@nams.kyushu-u.ac.jp*

^f*School of Transportation, Wuhan University of Technology, PR China,
e-mail: zhiyong-pei@whut.edu.cn*

Abstract

The present study focuses on buckling and collapse behaviors of cracked steel panel by accounting for the crack opening/closure. A rectangular panel with a transverse through crack to the loading direction is selected to better understand the typical mechanical characteristics of a panel subjected to a sequence of tensile to compressive loading. When a tensile load is applied to the cracked panel, a through crack gradually opened and yielding occurs around the crack tip. When a compressive load is applied after the tensile load, the crack gradually closed and elastic/elasto-plastic buckling occur. A shell-solid mixed finite element (FE) model is adopted to effectively analyze the crack opening/closure. Shell FEs are employed in the rectangular panel (shell model), while solid FEs are partially adopted around the crack (solid model). Double nodes and contact condition are imposed on the crack face. The shell and solid models are joined together with a rigid body element (RBE). The buckling and collapse behaviors of the panel models under a

*Corresponding author

sequence of tensile to compressive loading is critically examined, as well as its local behavior, *i.e.*, crack opening displacement (COD) varying displacement amplitude, panel aspect ratio and panel thickness. The results show that the crack opening/closure strongly affect the buckling and collapse behaviors of the cracked panel.

Keywords: Cracked Panel, Buckling, Collapse Behavior, Finite Element Method, Shell-Solid Modeling

1. Introduction

Ships and offshore structures are composed of steel structural members, *e.g.*, panel, stiffener and stiffened panel that are joined by welding [1]. The welded structures experience several sea states, and repetitive wave loads are applied to the structures. Previous studies have examined the ultimate strength of hull girders [2-5] and structural members [6-9] under several loading conditions. Such steel welded structures are prone to fatigue, fracture and corrosion damage. The buckling strength of the structural panels is normally accounted for in a structural design that considers corrosion allowance [10]. However, collapse accidents of ships sometime take place, especially on aged ships. Several studies have investigated the mechanical behaviors of cracked panel [11, 12], stiffened panel [13-18] and box/hull girders [19, 20]. Babazadeh and Khedmati provide a comprehensive review of collapse analysis of cracked ship structural elements and systems [21].

The buckling and collapse behaviors of cracked steel structural members involves several complicated and difficult mechanical problems such as geometrical/material nonlinearities, the influence of welding residual stress, crack tip damage evolution and crack closure. The authors have studied buckling problems [22-26] and fracture problems [27-29] employing meshfree method. Although fracture behavior of a cracked panel under a tensile load is frequently discussed, *e.g.*, [30-37], very few studies have investigated cracked panel behavior under compressive or cyclic load. Additionally, most studies have not considered the crack face contact. Further investigations are therefore required to appropriately understand and control structural damage in a fail-safe design of a ship's hull. Multiscale fatigue crack modeling in welded stiffened panels was recently reported [38] and the influence of welding residual stress on fatigue crack propagation was discussed [39]. Additionally, the ultimate residual strength of a ship's hull plate under uniaxial cyclic load has

been studied considering low-cycle fatigue damage to crack propagation [40].

In the present study, a cracked ship structural member subjected to a sequence of tensile to compressive loading is studied. A bottom panel of a ship with a transverse through crack to the loading direction is considered. It is assumed that the gap between the crack faces is initially very small compared with the panel thickness. When a tensile load is applied to the cracked steel panel, the crack gradually opened and yielding occurs around the crack tip. The gap increases under large loads and the crack tip may be blunted. When a compressive load is applied after the tensile load, elastic/elasto-plastic buckling may occur. The gap gradually closed and the crack faces may attach each other.

The buckling and collapse behavior of a cracked panel can differ from that of an intact panel. The behaviors also depends on whether the crack faces attach or not. A ship structural panel is normally modeled using shell FEs approach because the panel is very thin compared with the entire structure, but crack opening/closure is a localized phenomenon. Simultaneous simulation of these different scales using a standard shell FEs is difficult. Previous studies performed collapse analysis of a cracked stiffened panel employing shell FEs that considered the crack segment contact as a nonlinear spring [41, 42]. However, the full and partial contact of the crack face along the panel thickness direction cannot be modeled accurately.

A global-local analysis [43] is a numerical method that solves different scales of mechanical problems. Several numerical techniques have been proposed such as the zooming method [44], FE overlay technique [45-47] and perpendicular shell coupling method [48]. In this study, a shell-solid model, one of the analysis methods, is employed to effectively examine the mechanical behavior of the cracked panel by considering crack opening/closure. Shell FEs are employed within the entire panel and solid FEs are adopted in the crack segment. In a previous study, a surface crack in a cruciform welded joint was analyzed employing a shell-solid model with RBE3 [49] equipped with major commercial FE modeling software, *e.g.*, [51-54].

The investigation on the ultimate strength of a cracked panel under monotonic compressive loading using shell and shell-solid models have been carried out [50]. When a crack face contact is considered in an explicit method, the solution procedure can become unstable. The problems were then analyzed by dynamic explicit method employing LS-DYNA [51]. In the FE models, the gap between the crack faces is set to zero. The load carrying capacity of the cracked panels was carefully investigated for various crack lengths and

locations. Contact condition have been reported to be important for the buckling and collapse behaviors under compressive loading.

In the consideration of a real ship, the ship structural members are received tensile and compressive loading. A rectangular panel subjected to tensile and compressive loads is examined using the shell-solid model by accounting for the crack opening/closure. The crack is assumed to be stationary during loading. Although the present study focuses primarily on obtaining the general mechanical characteristics of a cracked panel subjected to a sequence of tensile to compressive loading, to the best of our knowledge, the cracked panel modeling and a discussion of buckling and collapse behavior have not been reported. The investigation is carried out to obtain the stress-strain curve and local behavior *i.e.* COD varying displacement amplitude, panel aspect ratio, and panel thickness.

The paper is organized as follows. The shell-solid model of a cracked panel is presented in Section 2. Buckling and collapse behaviors under monotonic compressive loading are discussed in Section 3. The behavior subjected to a sequence of tensile to compressive loading and crack opening/closure are presented in Section 4, and concluding remarks are given in Section 5.

2. Cracked panel modeling

2.1. Finite element model of a cracked panel

A schematic illustration of the modeling is shown in Fig.1(a). The whole structure is modeled by shell FEs (shell model) and the cracked section is modeled by solid FEs (solid model). The crack is modeled by double nodes. The shell and solid models are connected to each other with RBE3. The RBE3 develops a constraint relationship between the reference nodes in the shell model and the slave nodes in the solid model. The moment and force of the reference nodes are transferred to the slave nodes. An illustration of the FE model is shown in Fig.1(b). The RBE3 is included in commercial FE software, *e.g.*, LS-DYNA [51], NASTRAN [52] and ABAQUS [53]. Further details are provided in references and [18, 49].

LS-DYNA is chosen in the present computation. Element No.16 with a fully integrated element with four integration points is employed for the shell FEs. Element No.-2 is used as the solid FEs and is also a fully integrated element with eight integration points. A contact condition is imposed between the crack faces to model crack opening/closure. Friction between the crack

faces is neglected to better understand the typical mechanical characteristics of a panel subjected to a sequence of tensile to compressive loading.

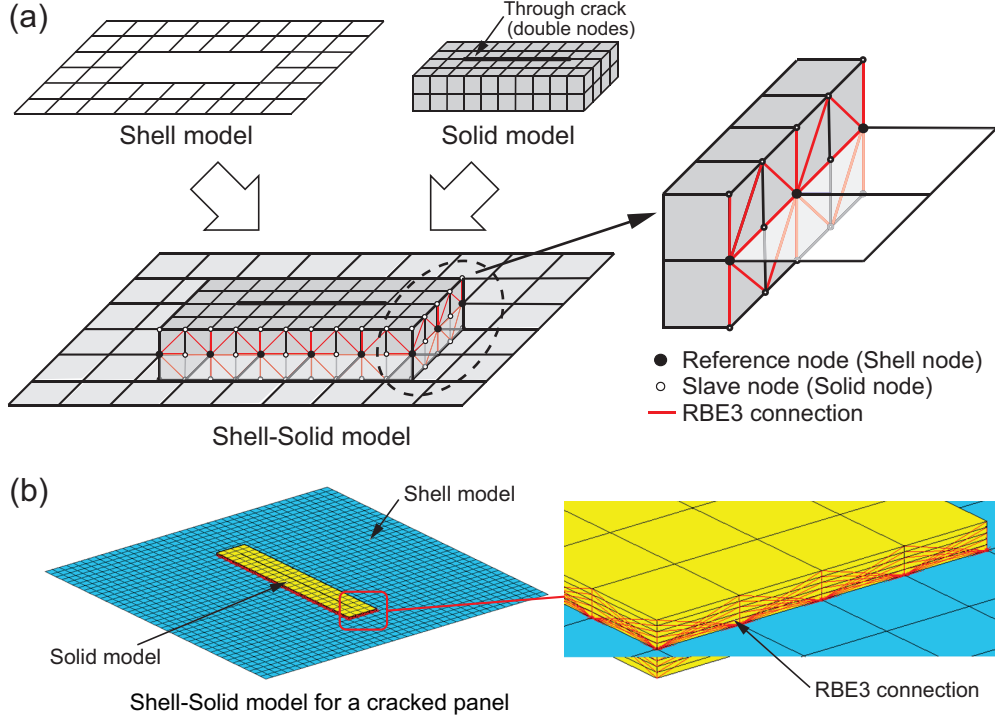


Figure 1: Shell-Solid modeling for a cracked panel employing RBE3. (a) Shell-Solid model. (b) Detail of the RBE3 connection.

2.2. Buckling and collapse analysis using the shell-solid model

A cracked rectangular panel is shown in Fig.2. The crack length and its position are illustrated in Fig.2(a). The panel size is $L_x \times L_y$ and the thickness is t . The crack is located in the middle span of the panel, *i.e.*, $l=L_x/2$ and its length is $2a$. The BCs and loading condition are shown in Fig.2(b). A simply supported condition is employed on all edges. The in-plane displacement of the edges in their perpendicular directions is assumed to be uniform by considering the continuity of plating by employing multiple point constraint (MPC). Uniaxial forced displacement is applied to one edge of the plate.

Two panel thickness $t=15$ and 20 mm, and three panel aspect ratio $\alpha=1$, 3 and 5 are employed for $2a=500$ mm to examine the influence of α and

t . Fig.2(c) shows a shell-solid model of $\alpha=1$ ($L_x=L_y=1,000$ mm). Whole the panel is modeled by shell FEs, while solid FEs are partially adopted around the crack part. The shell model is divided into 40 sections for the L_x and L_y directions, respectively, *i.e.*, the element size is 25×25 mm. The solid model dimensions include $w=100$ mm and $h=600$ mm. The element size is same with the shell element. Along the panel thickness direction, the solid model is divided into 10 sections for $t=15$ and 20 mm, respectively, as shown in Fig.1(b). The solid model size and division number of the FE model was determined in our previous study [50, 55]. The accuracy of shell-solid modeling has been carefully investigated in the literature using critical buckling loads and stress-strain curves, by changing the solid model size and division number of the FE model.

The shell-solid models with different α are shown in Fig.3. L_y is held at 1,000 mm and L_x changes in accordance with $\alpha=1, 3$ and 5, respectively. The element and solid model dimensions are fixed in all the models.

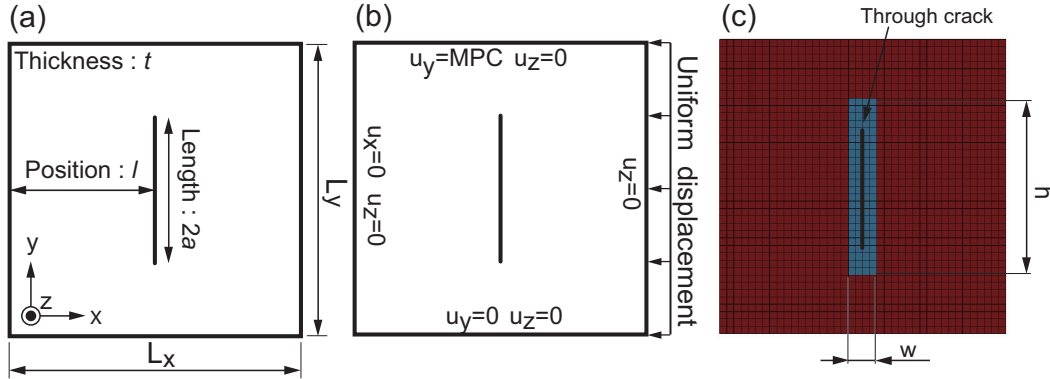


Figure 2: A cracked rectangular panel. (a) Crack length and position. (b) BCs and loading conditions. (c) Shell-solid model for $\alpha=1$.

2.3. Material properties and loading condition

Initial deflection 1, 3 and 5 half wave buckling modes are applied with a maximum deflection of 0.01 times that of the panel thickness for $\alpha=1, 3$ and 5, respectively. A mild steel is assumed with; Young's modulus $E=205,800$ MPa, Poisson's ratio $\nu=0.3$ and yield stress $\sigma_Y=313.6$ MPa. A schematic illustration of the stress-strain curve is given in Fig.4(a). A perfect elasto-plastic body is assumed because buckling behavior dominates and material hardening to the ultimate strength is relatively small.

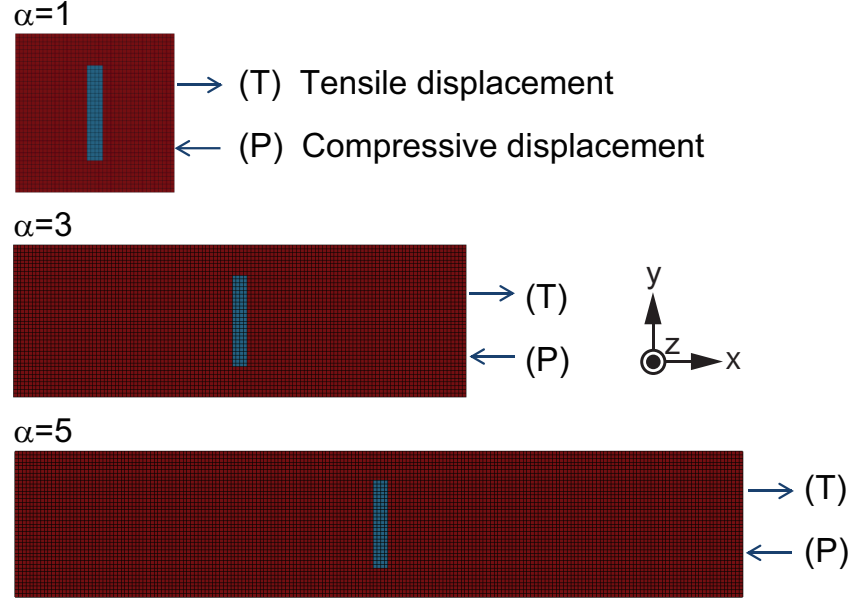


Figure 3: Tensile and compressive displacements are applied to the cracked panels with different $\alpha=1, 3$ and 5 .

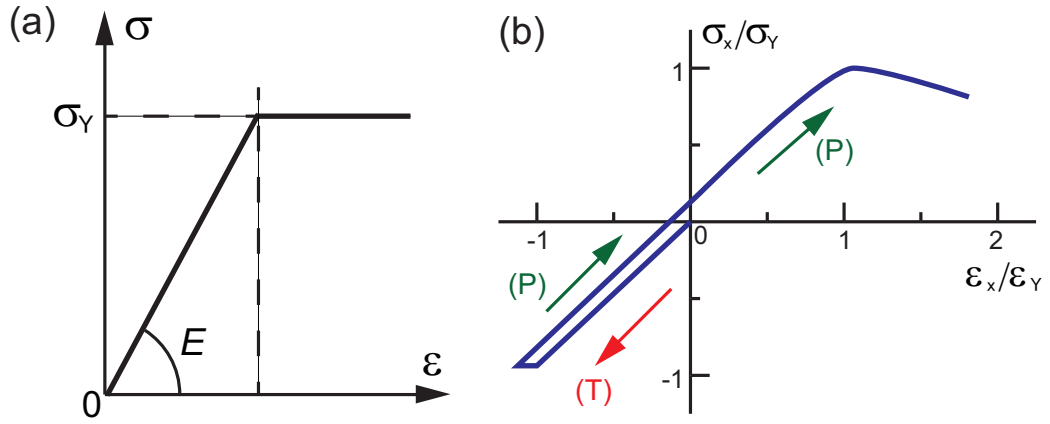


Figure 4: Schematic illustration of stress-strain curves for (a) Mild steel under tensile loading. (b) A panel subjected to a sequence of tensile to compressive loading.

Uniaxial forced displacement is applied and the reaction force is taken. Monotonic tensile displacement (T) is applied first, followed by monotonic compressive displacement (P) as shown in Fig.3. A schematic of the normalized stress-strain curve is presented in Fig.4(b). The horizontal axis shows normalized strain $\varepsilon_x/\varepsilon_Y$ and the vertical axis is normalized stress along the loading direction σ_x/σ_Y . $\varepsilon_x/\varepsilon_Y$ is negative for the tensile displacement, and positive for the compressive displacement. When uniform tensile and compressive displacements are respectively applied for different α and the entire the panel yields without buckling, the normalized strain is $\varepsilon_x/\varepsilon_Y = -1.0$ and 1.0 , respectively. $\varepsilon_x/\varepsilon_Y = -1.0$ and -2.0 are employed for the cracked panel analysis subjected to a sequence of tensile to compressive displacement.

3. Buckling and collapse analysis under monotonic compressive displacement

In this section, the description of cracked panel under monotonic compressive displacement is presented. The panel thickness is $t=15$ mm. The gap between the crack faces is set to zero. A crack face contact therefore occurs when the compressive stress is generated. The case for $\alpha=1$ [50] was previously examined and briefly reviewed the fundamentals here to get a basic knowledge of the cracked panel under compressive displacement. Buckling occurs in the intact case prior to reaching the ultimate strength.

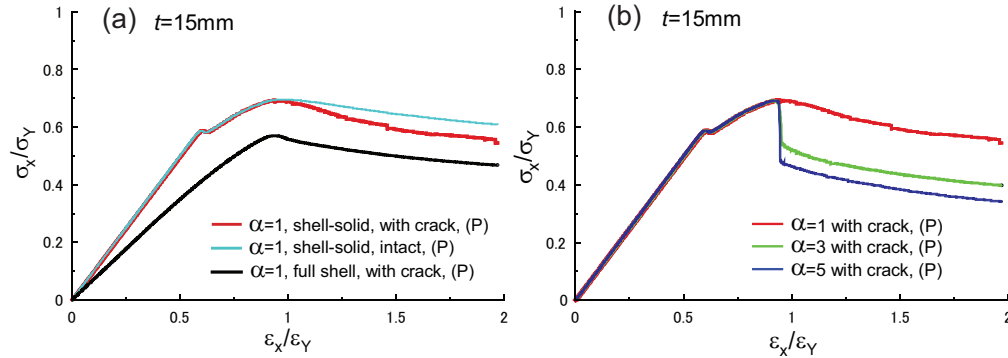


Figure 5: Stress-Strain curves for $t=15$ mm. (a) Intact and cracked panels for $\alpha=1$. (b) Cracked panels for $\alpha=1, 3$ and 5 .

The stress-strain curves of a cracked panel for $\alpha=1$ by employing shell-solid model are shown in Fig.5(a) and the result is compared with an intact

panel. Nearly identical load carrying capacities are observed prior to reaching the ultimate strength. With or without crack, the load is transferred due to the crack face contact. However, the load of the cracked panel decreases after reaching the ultimate strength. The crack face gradually slides and the contact area decreases along with out-of-plane deformation of the cracked panel.

Results of the shell-solid model are also compared with the full shell model for the cracked panel. The initial stiffness and ultimate strength of the shell model are lower than those of the shell-solid model because crack contact is neglected. The free surface cannot transfer the axial load.

Stress-strain curves for $\alpha=1, 3$ and 5 obtained from the cracked shell-solid models are shown in Fig.5(b). The same stiffness is observed just before reaching the ultimate strength, because the crack faces are almost attached and the axial load can be transferred. The load gradually decreases for $\alpha=1$ over the ultimate strength period, while an abrupt reduction is observed for $\alpha=3$ and 5 . Fig.6(a)-(c) show a cross-section of the cracked panel model for $\alpha=1, 3$ and 5 at the ultimate strength state. The contact area of the crack face remains for $\alpha=1$, while the crack surface moves rapidly and the contact area abruptly decreases for $\alpha=3$ and 5 along with out-of-plane deformation of the panel. The crack face contact and contact area affect the buckling and collapse behaviors of the cracked panels.

Deflection of the cracked panel during the post-ultimate strength state ($\varepsilon_x/\varepsilon_Y=1.5$), is shown in Fig.7(a)-(c) for $\alpha=1, 3$ and 5 , respectively. The deformation is enlarged five times for visualization. For $\alpha=1$, the roof mode is observed and the crack remains attached as shown in Fig.7(a). On the other hand, for $\alpha=3$ and 5 , the crack faces are almost separated and deformation localization is observed around the crack tip, as shown in Fig.7(b) and (c). The same trend is observed in the slope of the post-ultimate strength state for $\alpha=3$ and 5 as that shown in Fig.5(b). This is because the collapse region, *i.e.*, ligament of the cracked panel, has almost the same residual strength for the same $\varepsilon_x/\varepsilon_Y$. Although crack face friction is neglected for simplicity, these are typical examples of the buckling and collapse behavior of a cracked panel under compressive displacement.

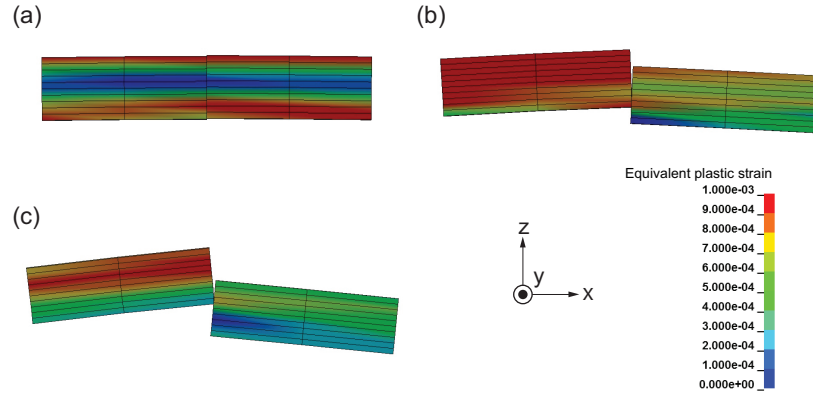


Figure 6: Cracked panel deformation at ultimate strength for $t=15$ mm (Equivalent plastic strain). (a) $\alpha=1$. (b) $\alpha=3$. (c) $\alpha=5$.

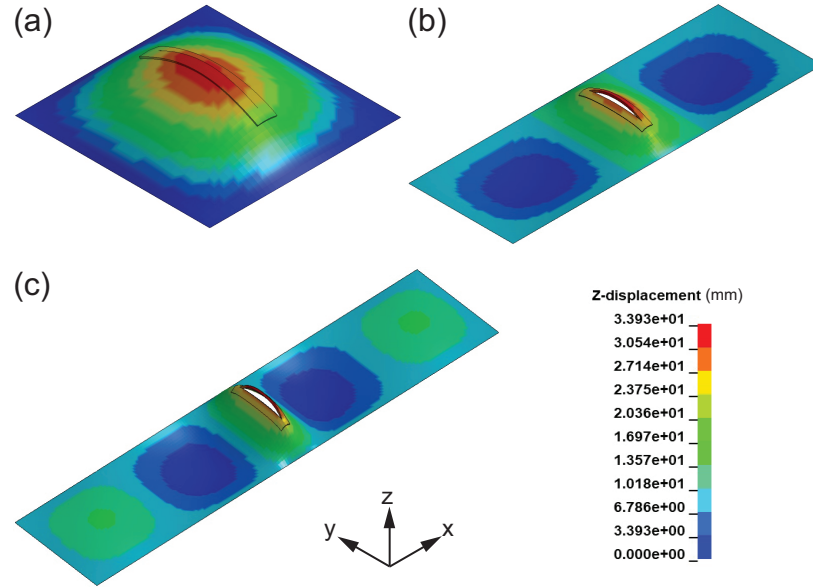


Figure 7: Deflection mode at the post-ultimate strength for $t=15$ mm (z -displacement, Deformation is enlarged five times). (a) $\alpha=1$. (b) $\alpha=3$. (c) $\alpha=5$.

4. Buckling and collapse analysis subjected to a tensile and compressive displacements

4.1. Cracked panel analysis subjected to a sequence of tensile to compressive displacement

A panel with $\alpha=1$ and $t=15$ mm is chosen. The stress-strain curves of intact and cracked panels using the shell-solid model are shown in Fig.8. The results with full shell model is also shown. In the figures, (T)-(P), 100% means that tensile displacement is applied until $\varepsilon_x/\varepsilon_Y=-1.0$ and compressive displacement is applied until reaching the post-ultimate strength state.

When tensile displacement is applied to the intact panel, the curve shows an elastic behavior as shown in Fig.8. The same path is therefore followed, even under compressive displacement as shown in Fig.5. Elasto-plastic behavior is observed for the cracked panel owing to the presence of a crack under tensile displacement. At point A in Fig.8, the panel undergoes the maximum tensile load, which is lower than the intact case. The stiffness changes at point B under the compressive displacement. The load increases and the panel attains the ultimate strength at point C. The load decreases at point D. Compared with the result of the full shell model in Fig.8, the curve under tensile displacement is the same as in the shell-solid model. On the other hand, the load is underestimated compared with results from the shell-solid model under compressive displacement.

To further investigate the buckling and collapse behaviors, COD is analyzed. COD is defined as the distance between two nodes across the crack face along the middle-plane (mid-plane) of the panel. The COD results are shown in Fig.9. Under tensile displacement, the shell-solid and shell model results are same, while the COD of the shell model becomes negative under compressive displacement. This means that crack faces of the shell model cross and overlap. On the other hand, crack closure is observed in the shell-solid model. The effectiveness of shell-solid modeling is verified for realistic discussion of the buckling and collapse behavior of a cracked panel under compressive displacement.

Contour diagrams of a cracked panel are shown in Fig.10(a)-(d) that correspond to points A to D in Fig.8, respectively. There are von Mises stresses on the top surface of the panel. When tensile displacement is applied, stress concentrates around the crack tip. When approaching the peak tensile load at point A, the crack tip region gradually yields as shown in Fig.10(a). After the peak, the load decrease under compressive displacement. Even

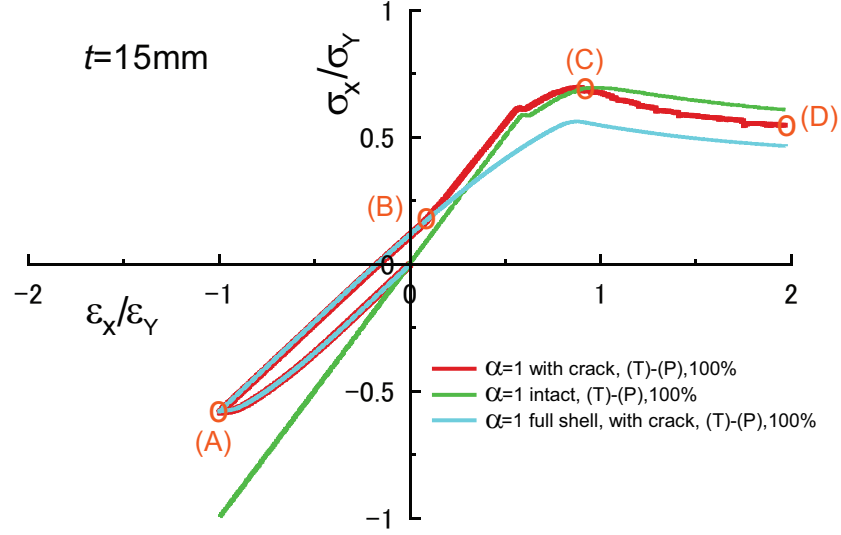


Figure 8: Stress-Strain curves subjected to a sequence of tensile to compressive displacement for intact and cracked panels.

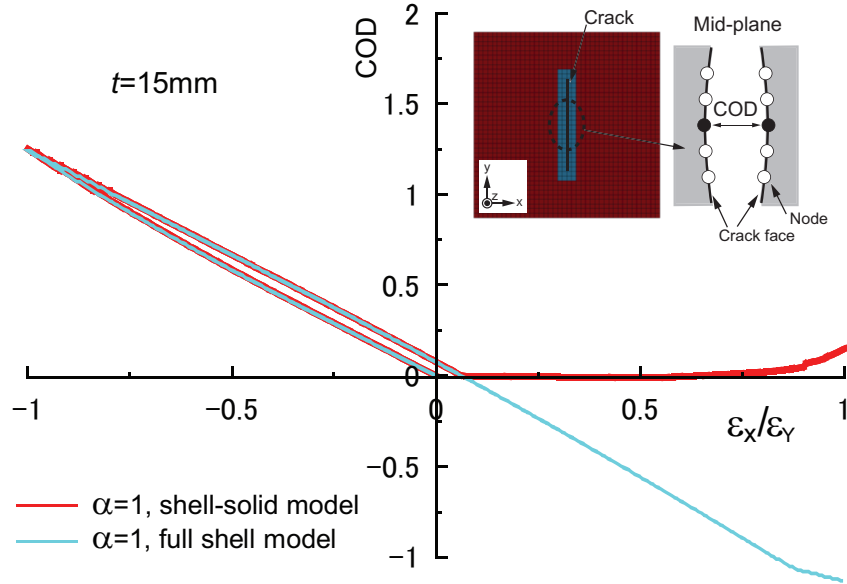


Figure 9: COD for cracked shell and shell-solid models subjected to a sequence of tensile to compressive displacement, $t=15\text{ mm}$.

for $\varepsilon_x/\varepsilon_Y=0.0$, the crack remains open and σ_x/σ_Y is positive because of the presence of plastic strain around the crack tip as shown in Figs.8 and 9. The crack face is attached at point B, and the stiffness increases relative to the full shell model. The stress distribution is shown in Fig.10(b). The panel reaches the ultimate strength at point C and the contour is shown in Fig.10(c). Beyond the ultimate strength, the load decreases at point D. The contour is shown in Fig.10(d).

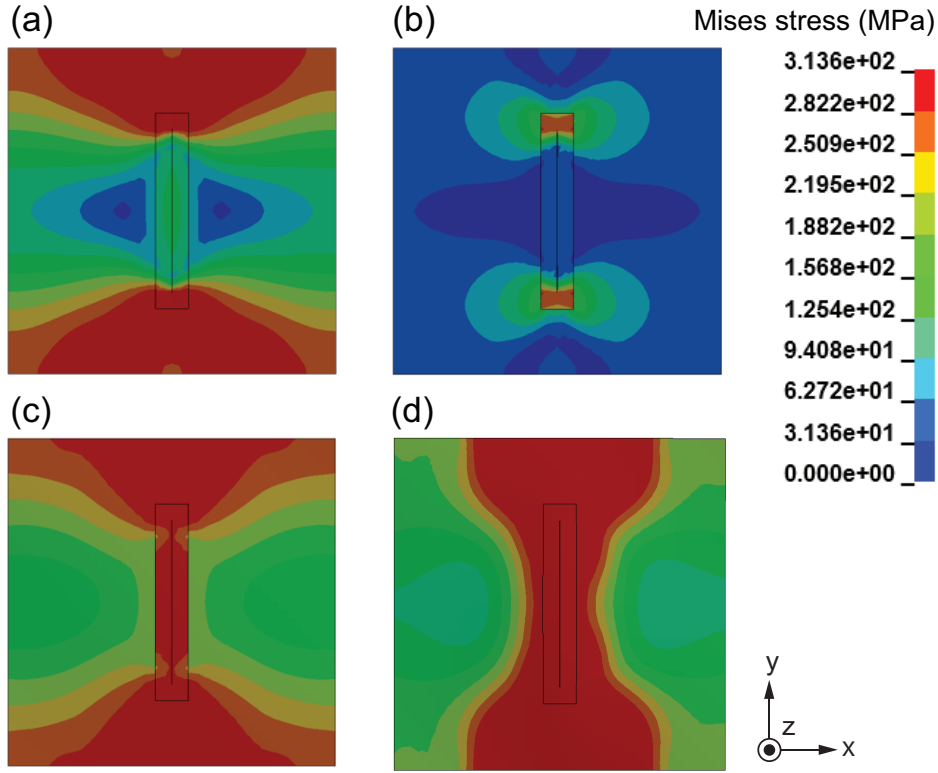


Figure 10: Contour diagram of the stress distribution on the top of panel (Mises stress). (a) Maximum tension. (b) Crack contact. (c) Ultimate strength. (d) Post-ultimate strength.

The plastic strain distribution at the top of the panel is shown in Fig.11(a) and (b). Deformation at maximum tension, *i.e.*, $-\varepsilon_x/\varepsilon_Y=1.0$, is shown in Fig.11(a). The plastic strain distribution is non-uniform owing to existence of the crack. Stresses concentrate and the yield region expands around the crack tip. The panel stiffness also reduces because of the crack, relative to the intact case. Under the maximum tensile load, the COD is approximately

1.25 mm as shown in Fig.9. A crack face contact occurs and σ_x/σ_Y increases at point B in Fig.8 for $\varepsilon_x/\varepsilon_Y=0.06$. The deformation and plastic strain distribution is shown in Fig.11(b).

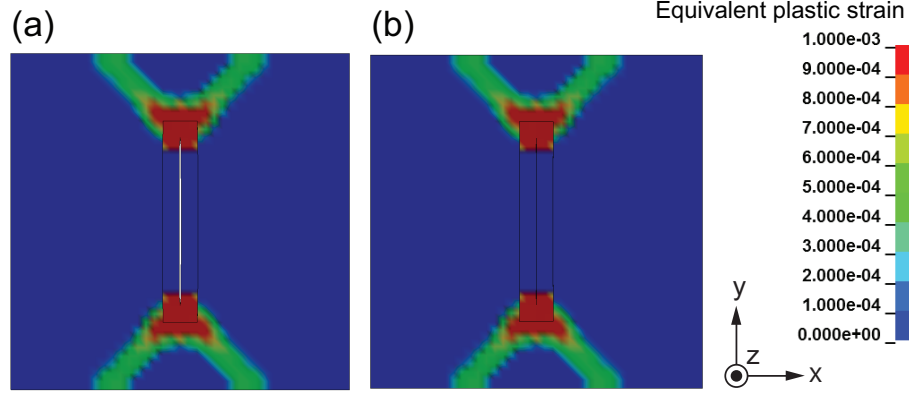


Figure 11: Equivalent plastic strain distribution on the top of the panel, $t=15$ mm. (a) Opening crack at $-\varepsilon_x/\varepsilon_Y=1.0$. (b) The crack is closed at $\varepsilon_x/\varepsilon_Y=0.06$.

4.2. Effect of forced displacement amplitude

In this section, the buckling and collapse behaviors of the cracked panel for different forced displacements are examined. A panel for $\alpha=1$ and $t=15$ mm is used. Tensile displacements of 100% and 200% of the yield strain *i.e.*, $\varepsilon_x/\varepsilon_Y=-1.0$ and $\varepsilon_x/\varepsilon_Y=-2.0$ are imposed respectively. Compressive displacement is then applied until the post-ultimate strength. These are defined as (T)-(P), 100% and (T)-(P), 200%, respectively. The problems are analyzed using the shell-solid model. The stress-strain curves and CODs are presented in Figs.12 and 13.

As shown in Fig.12, points E-H represent the (T)-(P), 200% curve. For reference, points A-D for (T)-(P), 100% are also shown. Tensile displacement is applied until $\varepsilon_x/\varepsilon_Y=-2.0$, and the maximum tensile load occurs at point E. The COD at the maximum tensile displacement is shown in Fig.13. The COD path and crack opening/closure behavior are different with (T)-(P), 100%. The plastic strain distribution at the maximum tensile load is shown in Fig.14(a). In addition to an increase of tensile load, the yield region and plastic strain around the crack tip also expand. The maximum COD of (T)-(P), 200% is almost two times greater than that of (T)-(P), 100%.

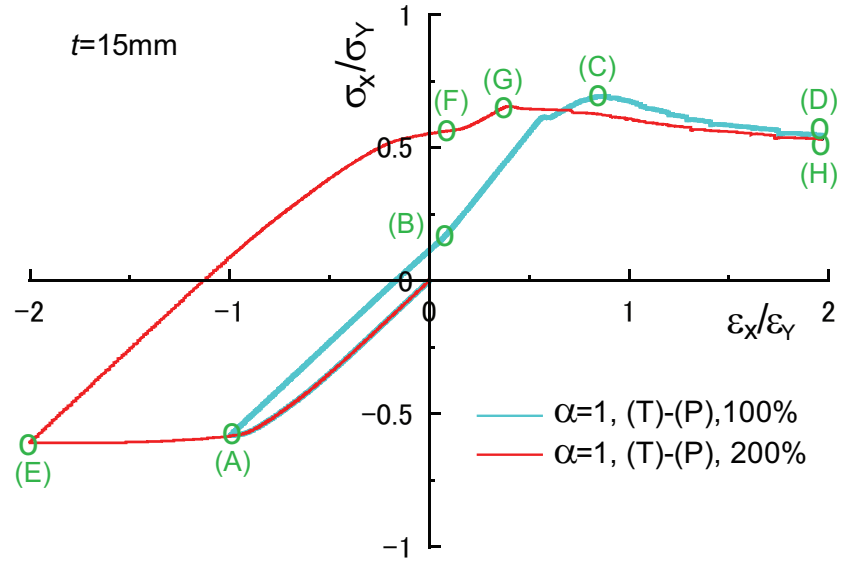


Figure 12: Stress-Strain curves for different forced displacements.

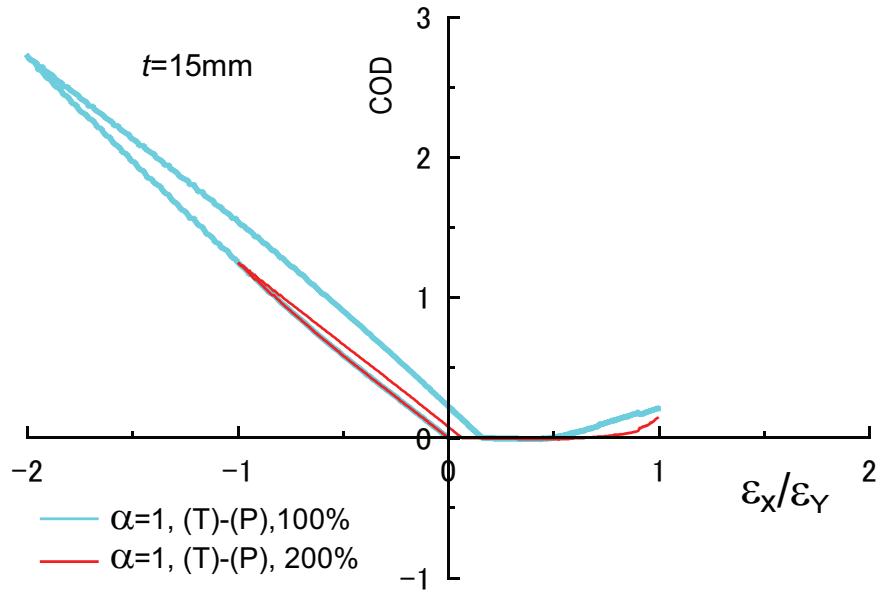


Figure 13: CODs for different forced displacements.

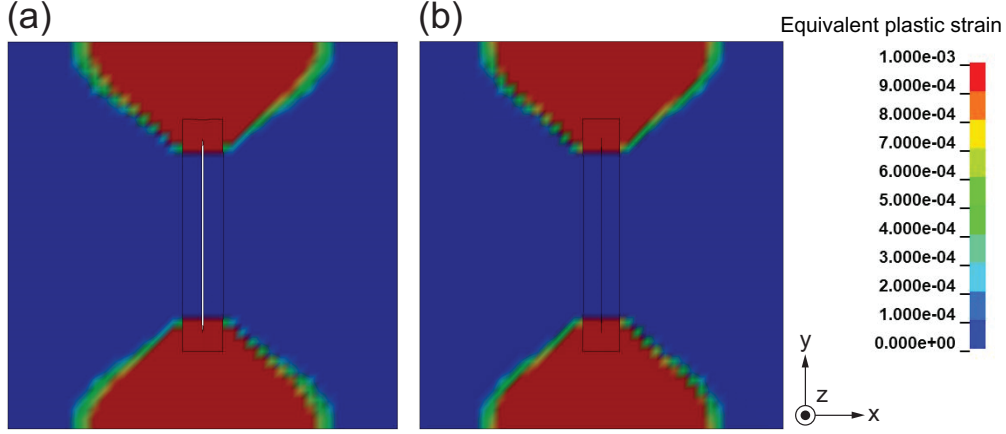


Figure 14: Equivalent plastic strain distribution on the top of the panel, $t=15$ mm. (a) Opening crack at $-\varepsilon_x/\varepsilon_Y=2.0$. (b) The crack is closed at $\varepsilon_x/\varepsilon_Y=0.17$.

The load and COD decrease after peak tensile displacement. As well as in (T)-(P), 100%, the crack is still open even when $\varepsilon_x/\varepsilon_Y=0.0$ as shown in Fig.13. At point F, the crack faces become attached at $\varepsilon_x/\varepsilon_Y=0.17$. The crack closure behavior and plastic strain distribution are shown in Fig.14(b). After the crack face contact, the load increases slightly and the panel reaches the ultimate strength at point G. The load then decreases as $\varepsilon_x/\varepsilon_Y$ increases at point H. Because the yield region expands and plastic strain increases, the ultimate strength is lower than (T)-(P), 100% and the intact case as shown in Fig.8.

4.3. Effect of panel aspect ratio

The buckling and collapse behavior of the cracked panel is examined for different α . $\alpha=1, 3$ and 5 are employed for $t=15$ mm. (T)-(P), 100% is chosen for the tensile displacement. The stress-strain curves are shown in Fig.15 and the CODs for different α are shown in Fig.16.

At maximum tensile displacement $\varepsilon_x/\varepsilon_Y=-1.0$, nearly same load is observed at point A for different α . Under compressive displacement, the crack attaches at points B and C for $\alpha=1$ and 3 , respectively. The crack closure for $\alpha=1$ and 3 can be seen in Fig.16. The closure occurs before the ultimate strength for $\alpha=1$, while it occurs around the ultimate strength for $\alpha=3$. For $\alpha=5$, after the ultimate strength, the COD of the mid-plane reaches a minimum value around $\varepsilon_x/\varepsilon_Y=0.45$ at point D, but nodes in the mid-plane do not attach each other as shown "α=5, mid-plane" in Fig.16.

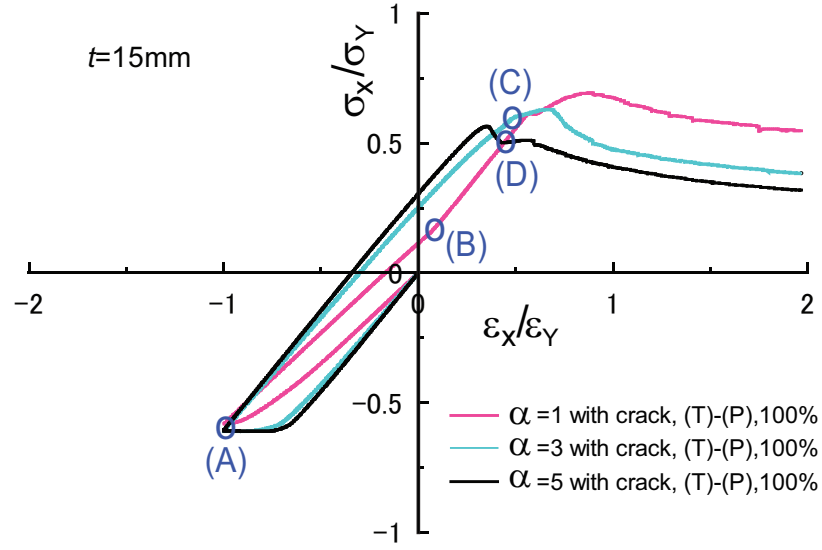


Figure 15: Stress-Strain curve for $\alpha=1, 3$ and 5 .

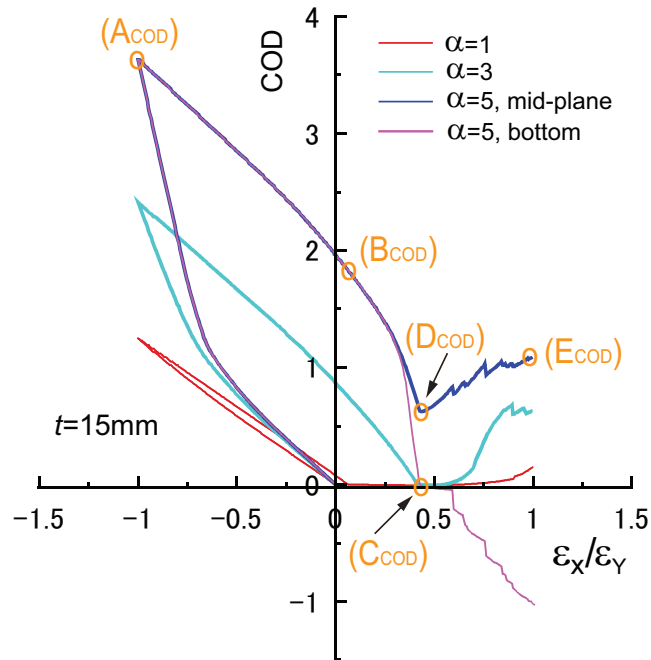


Figure 16: CODs for $\alpha=1, 3$ and 5 .

The COD at the bottom of the panel is defined to further investigate the behavior of $\alpha=5$. This is also shown in Fig.16 as " $\alpha=5$, bottom" and deformation around the crack is shown in Fig.17. Fig.17(a)-(e) correspond to the timing of points A_{COD}-E_{COD} in Fig.16, respectively. The crack opens under maximum tensile load at point A_{COD}. The COD gradually closes under compressive displacement at point B_{COD}. The bottom of the panel attaches at point C_{COD} once the panel reaches its ultimate strength. After attachment, the crack faces slides with out-of-plane deformation of the panel at point D_{COD}. Substantial deformation occurs around the crack at point E_{COD}. The panel therefore reaches the ultimate strength without contacting the crack face.

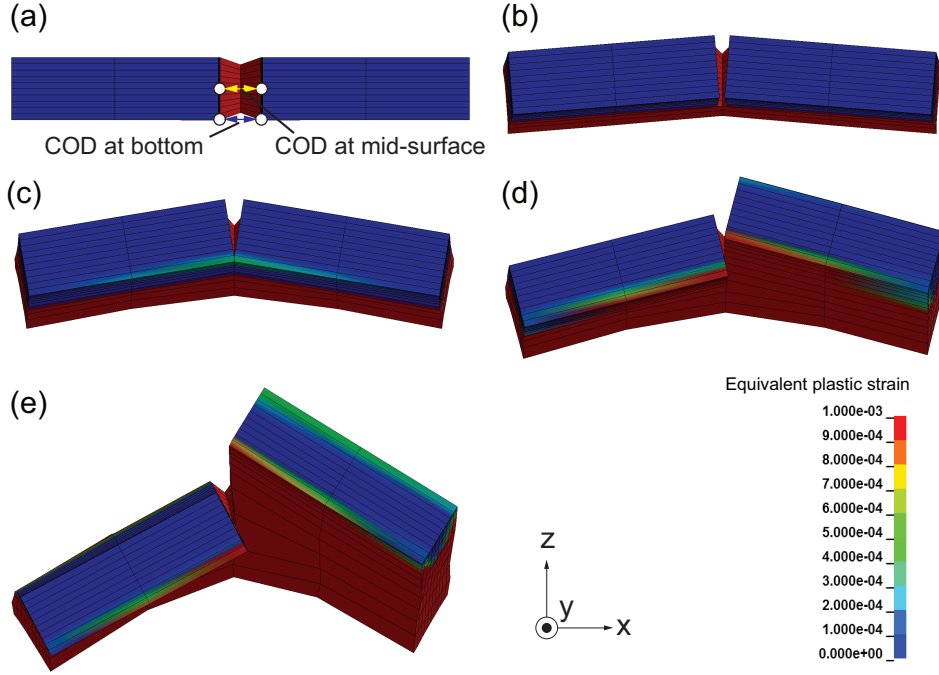


Figure 17: Deformation of the cracked panel for $\alpha=5$ along cross-section (Deformation is enlarged five times) at different points. (a) A_{COD}. (b) B_{COD}. (c) C_{COD}. (d) D_{COD}. (e) E_{COD}.

The plastic strain distribution at $\varepsilon_x/\varepsilon_Y=-1.0$ for $\alpha=3$ and 5 is shown in Fig.18(a) and (b), respectively, and in Fig.11(a) for $\alpha=1$. Localized deformation occurs around the crack under tensile displacement, while the external region remains elastic. Stiffness decreases when α is small, because the yield-

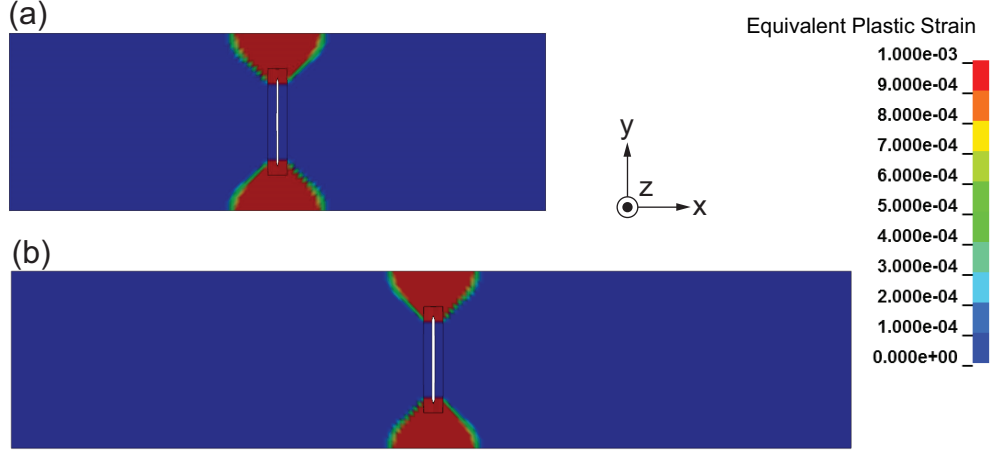


Figure 18: Plastic strain distribution on the top of the panel at maximum tension $t=15$ mm. (a) $\alpha=3$, (b) $\alpha=5$.

ing region extends relative to the entire panel. When α is larger, the stiffness is relatively high under both tensile and compressive displacement as shown in Fig.15. However, the maximum COD becomes large because deformation is localized around the crack. The crack tip is blunted during tensile displacement because the plastic region is larger. As a result, crack closure is delayed or the crack continues to open under the compressive load. Additionally, the panel reaches the ultimate strength without crack closure, *e.g.*, $\alpha=5$. For $\alpha=1, 3$ and 5 , the ultimate strength decreases as α increase.

4.4. Effect of panel thickness

The effect of panel thickness is examined using $t=20$ mm for $\alpha=1, 3$ and 5 and loading conditions of (P), (T)-(P), 100% and (T)-(P), 200%, respectively. The intact panel model is also examined for comparison.

The stress-strain curve of the intact panel for $\alpha=1$ is shown in Fig.19 alongside results of (P) and (T)-(P), 100%. When buckling occurs prior to reaching the ultimate strength under compressive displacement for $t=15$ mm, buckling deformation is limited to $t=20$ mm until collapse because the critical buckling load increases with panel thickness. Because no yielding occurs until $\varepsilon_x/\varepsilon_Y=-1.0$, the same path is taken for (P) and (T)-(P), 100% using the intact panel.

The stress-strain curve of the cracked panel with $\alpha=1$ is shown in Fig.20. The CODs of the cracked panel are shown in Fig.21. Under conditions of

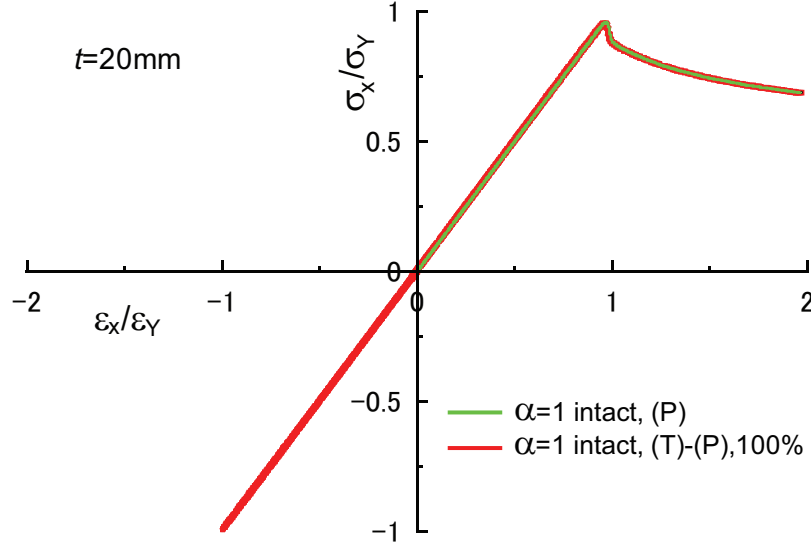


Figure 19: Stress-Strain curves for an intact panel, $t=20$ mm.

monotonic compressive displacement (P), the ultimate strength and load carrying capacity are nearly the same as with the intact case as shown in Fig.19, because the crack face attaches during compression. The load gradually decreases after reaching the ultimate strength compared with the intact case owing to decreased contact area of the crack surface. The curves under tensile to compressive displacement (T)-(P), 100% and (T)-(P), 200% are presented for points A-D and points E-H, respectively. The curves and CODs show similar behaviors in the case of $t=15$ mm, as shown in Fig.12.

The deflection mode of the cracked panel is shown in Fig.22 for (T)-(P), 200%. Fig.22(a)-(c) correspond to points F-H in Fig.20, respectively. The crack tip is blunted owing to the large tensile load. At point F, only the center part of the surface crack is attached. The contact area gradually increases with increasing compressive displacement, and the panel reaches the ultimate strength at point G. Beyond that point, the contact area of the crack gradually decreases alongside out-of-plane deformation of the cracked panel. This behavior can be observed for $t=15$ mm, however, the crack face attaches near the ultimate strength as shown in points F to G in Fig.12.

The stress-strain curves and CODs for different α are shown in Figs.23 and 24, respectively. The behavior under tensile displacement is practically the same as for $t=15$ mm and similar maximum tensile loads are obtained at

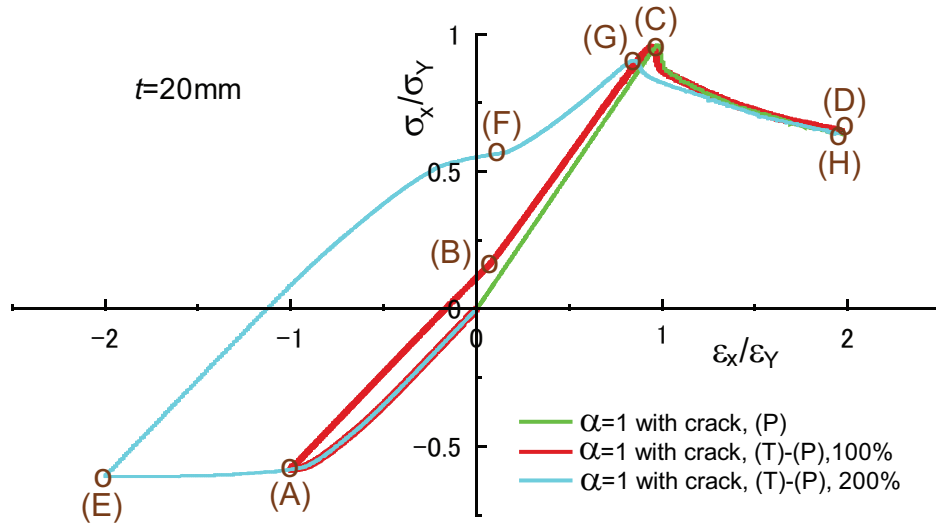


Figure 20: Stress-Strain curves for a cracked panel, $t=20\text{ mm}$.

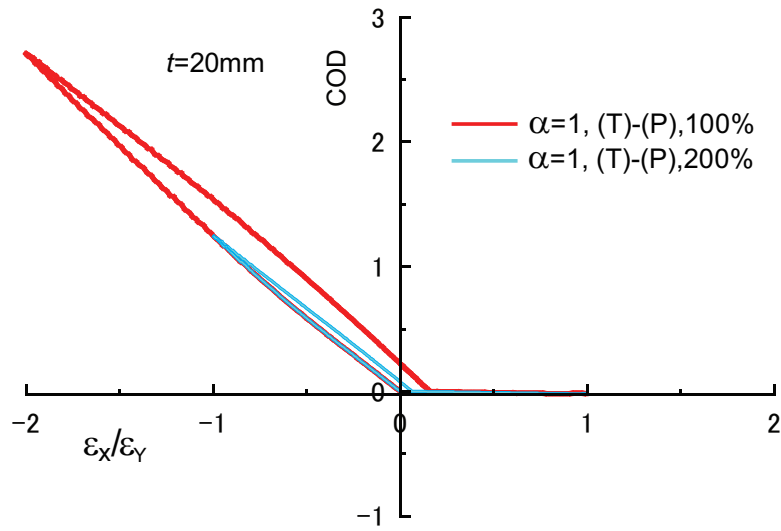


Figure 21: COD for cracked panels for (T)-(P), 100% and (T)-(P), 200%, $t=20\text{ mm}$.

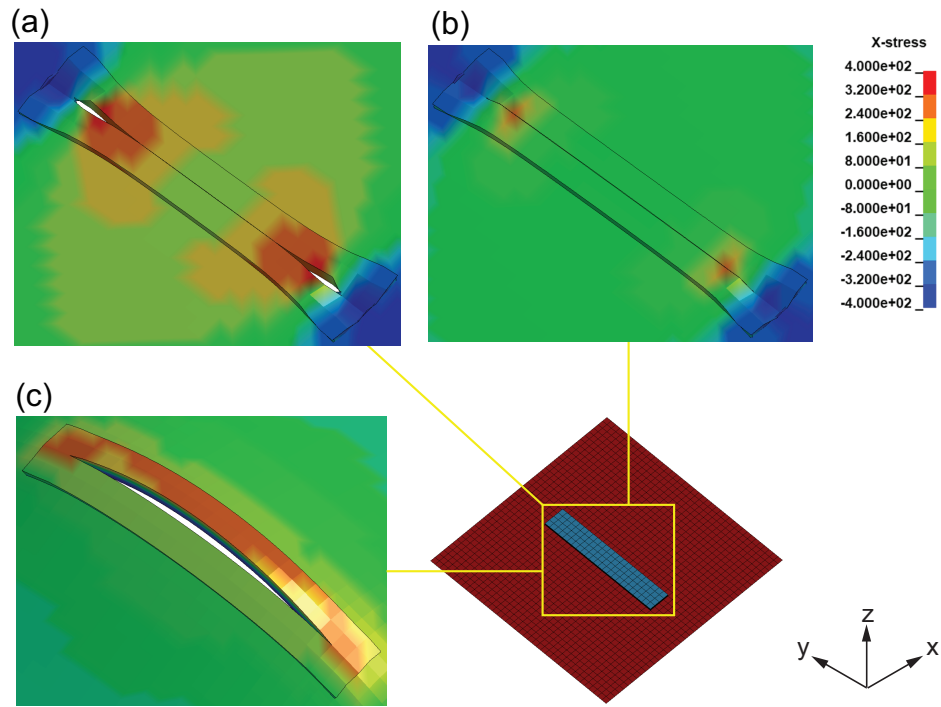


Figure 22: Deflection mode of the cracked panel during compressive displacement, $t=20$ mm, (T)-(P), 200% (Deformation is enlarged five times) (a) At point F. (b) At point G. and (c) At point H.

point A for all α investigated. During compressive displacement, the crack face contact occurs at points B, C and D, for $\alpha=1, 3$ and 5, respectively. After contacting the crack face, the same stiffness is observed for different α until reaching the ultimate strength. The ultimate strength is lower with increasing α .

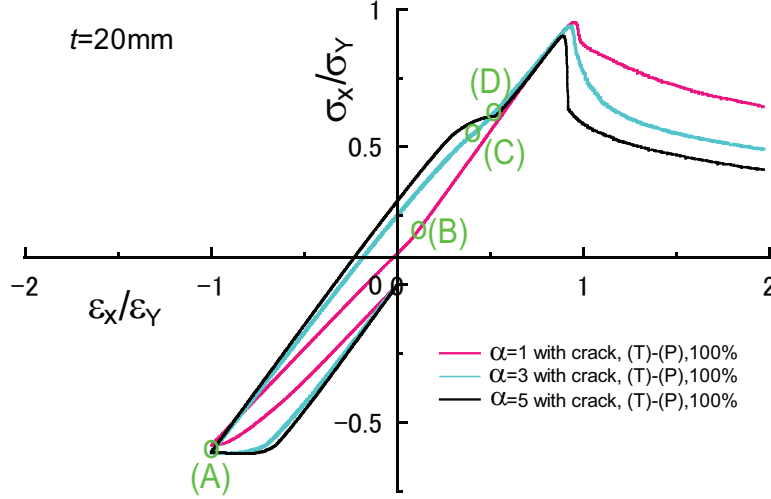


Figure 23: Stress-Strain curve of the cracked panels with different α , $t=20$ mm.

5. Conclusion

Buckling and collapse behaviors of a cracked steel panel subjected to a sequence of tensile to compressive loading are investigated by accounting for the opening and closing of cracks using a shell-solid modeling. A contact condition is assumed for the crack faces. A rectangular panel with a transverse through crack is chosen to understand the typical mechanical characteristics of the cracked panel. The normalized stress-strain curves and CODs varying displacement amplitudes, panel aspect ratios and panel thickness have been examined.

The cracked panel and shell-solid modeling is presented in Section 2, as well as the material properties and loading conditions. In section 3, the buckling and collapse behavior of the cracked panel under monotonic compressive displacement is discussed. The stress-strain curves of cracked and intact panels during compressive displacement are practically identical prior

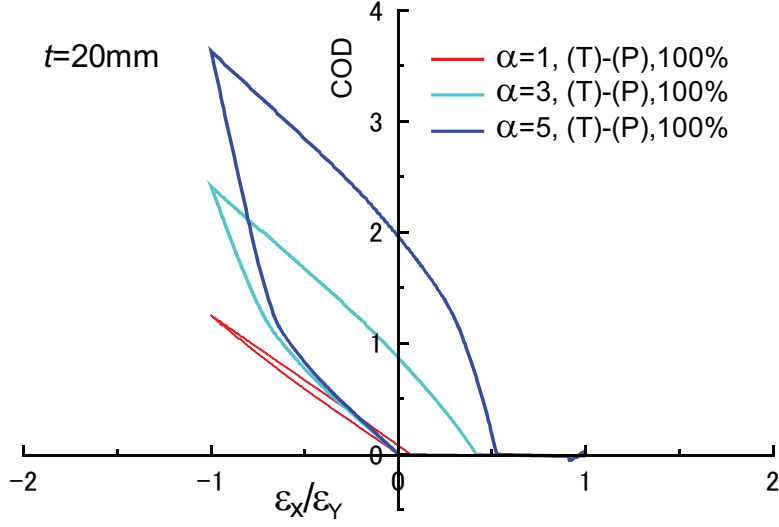


Figure 24: CODs for different α , $t=20$ mm.

to reaching the ultimate strength because the crack attaches and the axial load is transferred. After reaching the ultimate strength, the crack face slides, contact area decreases, and the load of the cracked panel gradually decreases compared with the intact case.

The cracked panel behavior subjected to a sequence of tensile to compressive loading is examined in Section 4 using variable displacement amplitude, panel aspect ratio and panel thickness. Under tensile loading, the crack opens and plastic strain is generated around the crack tip. Under compressive displacement, crack closure is delayed owing to the plastic deformation. The stiffness recovers once the crack face is attached because the axial load is transferred through the contact area. Beyond the ultimate strength, the crack face slides and the load decreases. The COD and plastic strain increase with displacement amplitude. Crack closure is also delayed owing to the large yield region. The COD and plastic strain also increase with increasing aspect ratio. In some cases, the panel reaches the ultimate strength without attachment of the crack face. The ultimate strength decreases with increasing displacement amplitude and aspect ratio. Plate behavior is similar for scenarios with larger plate thickness and $t=15$ mm, however, buckling deformation is limited to $t=20$ mm for collapse owing to the plastic deformation as also observed in the case of an intact panel.

In this study, it is assumed that the crack is stationed to understand

typical mechanical characteristics of a cracked panel under a sequence of tensile and compressive load. And, it is reported that the stiffness of the plate recovers when the crack contacts. When considering a real cracked structure, especially under tensile and compressive cyclic loading, damage at crack tip evolves and the crack will be extended. In such case, it is considered that not only the stiffness but also the ultimate strength will be reduced. As a future study, experimental and numerical studies for cracked panel under cyclic loading will be carried out to clarify the damaging process.

Acknowledgements

The authors thank to Shuhei Shinkawa (Graduate School of Engineering, Hiroshima University) for valuable comments on this study. This research was partially supported by the JSPS Grants-in-Aid for Scientific Research (C)(15K06632).

References

- [1] T. Yao, M. Fujikubo, Buckling and ultimate strength of ship and ship-like floating structures, first *ed.*, Butterworth-Heinemann-Elsevier, 2016.
- [2] T. Yao, O.C. Astrup, P. Caridis, Y.N. Chen, S.R. Cho, R.S. Dow, O. Niho, P. Rigo, Ultimate hull girder strength, Proc. of the 14th International Ship and Offshore Structures Congress (ISSC 2000) 321-391.
- [3] T. Yao, Hull girder strength, Mar. Struct. 16(2003) 1-13.
- [4] Z. Pei, K. Iijima, M. Fujikubo, S. Tanaka, S. Okazawa, T. Yao, Simulation on progressive collapse behaviour of whole ship model under extreme waves using idealized structural unit method, Mar. Struct. 40(2015) 104-133.
- [5] Z. Pei, K. Iijima, M. Fujikubo, Y. Tanaka, S. Tanaka, S. Okazawa, T. Yao, Collapse behaviour of a bulk carrier under alternate heavy loading conditions, Int. J. Offshore. Polar. Eng. 23(2013) 232-239.
- [6] M. Fujikubo, T. Yao, M.R. Khedmati, M. Harada, D. Yanagihara, Estimation of ultimate strength of continuous stiffened panel under combined transverse thrust and lateral pressure Part 1: Continuous plate, Mar. Struct. 18(2005) 383-410.

- [7] M. Fujikubo, M. Harada, T. Yao, M.R. Khedmati, D. Yanagihara, Estimation of ultimate strength of continuous stiffened panel under combined transverse thrust and lateral pressure Part 2: Continuous stiffened panel, *Mar. Struct.* 18(2005) 411-427.
- [8] S. Tanaka, D. Yanagihara, A. Yasuoka, M. Harada, S. Okazawa, M. Fujikubo, T. Yao, Evaluation of ultimate strength of stiffened panels under longitudinal thrust, *Mar. Struct.* 36(2014) 21-50.
- [9] M. Ozdemir, A. Ergin, D. Yanagihara, S. Tanaka, T. Yao, A new method to estimate ultimate strength of stiffened panels under longitudinal thrust based on analytical formulas. *Mar. Struct.* 59(2018) 510-535.
- [10] IACS, Common structural rules for bulk carriers and oil tankers (IACS CSR BC & OT), International Association of Classification Societies (2017).
- [11] M.R. Khedmati, P. Edalat, M. Javidruzi, Sensitivity analysis of the elastic buckling of cracked plate elements under axial compression, *Thin-Walled Struct.* 47(2009) 522-536.
- [12] J.K. Paik, Y.V.S. Kumar, J.M. Lee, Ultimate strength of cracked plate elements under axial compression or tension, *Thin-Walled Struct.* 43(2005) 237-272.
- [13] J.K. Paik, Residual ultimate strength of steel plates with longitudinal cracks under axial compression - Nonlinear finite element method investigations, *Ocean Eng.* 36(2009) 266-276.
- [14] X.H. Shi, J. Zhang, C.G. Soares, Experimental study on collapse of cracked stiffened plate with initial imperfections under compression, *Thin-Walled Struct.* 114(2017) 39-51.
- [15] M.C. Xu, Y. Garbatov, C.G. Soares, Residual ultimate strength assessment of stiffened panels with locked cracks, *Thin-Walled Struct.* 85(2014) 398-410.
- [16] C. Cui, P. Yang, C. Li, T. Xia, Ultimate strength characteristics of cracked stiffened plates subjected to uniaxial compression, *Thin-Walled Struct.* 113(2017) 27-38.

- [17] C. Yu, Y.T. Chen, S. Yang, Y. Liu, G.C. Lu, Ultimate strength characteristic and assessment of cracked stiffened panel under uniaxial compression, *Ocean Eng.* 152(2018) 6-16.
- [18] Y. Setoyama, D. Yanagihara, S. Tanaka, K. Taniguchi, Investigation of residual ultimate strength for stiffened panel structure with crack damage under uni-axial thrust, *J. Jpn. Soc. Naval Arch. Ocean Eng.* 28(2018) 75-88. (in Japanese).
- [19] J.K. Paik, Residual ultimate strength of steel plates with longitudinal cracks under axial compression - experiments, *Ocean Eng.* 35(2008) 1775-1783.
- [20] D.W. Gao, G.J. Shi, D.Y. Wang, Residual ultimate strength of hull structures with crack and corrosion damage, *Eng. Fail. Anal.* 25(2012) 316-328.
- [21] A. Babazadeh, M.R. Khedmati, Ultimate strength of cracked ship structural elements and systems: A review, *Eng. Fail. Anal.* 89(2018) 242-257.
- [22] S. Sadamoto, S. Tanaka, S. Okazawa, Elastic large deflection analysis of plates subjected to uniaxial thrust using meshfree Mindlin-Reissner formulation, *Comput. Mech.* 52(2013) 1313-1330.
- [23] S. Sadamoto, M. Ozdemir, S. Tanaka, K. Taniguchi, T.T. Yu, T.Q. Bui, An effective meshfree reproducing kernel method for buckling analysis of cylindrical shells with and without cutouts, *Comput. Mech.* 59(2017) 919-932.
- [24] S. Sadamoto, S. Tanaka, K. Taniguchi, M. Ozdemir, T.Q. Bui, C. Murakami, D. Yanagihara, Buckling analysis of stiffened plate structures by an improved meshfree flat shell formulation, *Thin-Walled Struct.* 117(2017) 303-313.
- [25] M. Ozdemir, S. Sadamoto, S. Tanaka, S. Okazawa, T.T. Yu, T.Q. Bui, Application of 6-DOFs meshfree modeling to linear buckling analysis of stiffened plates with curvilinear surfaces, *Acta Mech.* 229(2018) 4995-5012.

- [26] M. Ozdemir, S. Tanaka, S. Sadamoto, T.T. Yu, T.Q. Bui, Numerical buckling analysis for flat and cylindrical shells including through crack employing effective reproducing kernel meshfree modeling, *Eng. Anal. Bound. Elem.* 97 (2018) 55-66.
- [27] S. Tanaka, H. Suzuki, S. Sadamoto, M. Imachi, T.Q. Bui, Analysis of cracked shear deformable plates by an effective meshfree plate formulation, *Eng. Fract. Mech.* 144(2015) 142-157.
- [28] S. Tanaka, H. Suzuki, S. Sadamoto, S. Sannomaru, T.T. Yu, T.Q. Bui, *J*-integral evaluation for 2D mixed-mode crack problems employing a meshfree stabilized conforming nodal integration method, *Comput. Mech.* 58(2016) 185-198.
- [29] S. Tanaka, H. Suzuki, S. Sadamoto, S. Okazawa, T.T. Yu, T.Q. Bui, Accurate evaluation of mixed-mode intensity factors of cracked shear deformable plates by an enriched meshfree Galerkin formulation, *Arch. Appl. Mech.* 87(2017) 279-298.
- [30] W. Fricke, Fatigue analysis of welded joints: state of development, *Mar. Struct.* 16(2003) 185-200.
- [31] S. Suresh, Fatigue of materials, 2nd *ed.*. Cambridge University Press, Cambridge, United Kingdom, 1998.
- [32] T.L. Anderson, Fracture mechanics: Fundamentals and applications 3rd *ed.*. CRC Press, United Kingdom, 2005.
- [33] S.J. Maddox, Fatigue strength of welded structures, 2nd *ed.*. Woodhead Publishing, Cambridge, United Kingdom, 1991.
- [34] Y. Sumi, Fatigue crack propagation and computational remaining life assessment of ship structures, *J. Mar. Sci. Tech.* 3(1998) 102-112.
- [35] T. Okawa, Y. Sumi, M. Mohri, Simulation-based fatigue crack management of ship structural details applied to longitudinal and transverse connections, *Mar. Struct.* 19(2006) 217-240.
- [36] R. Gadallah, N. Osawa, S. Tanaka, S. Tsutsumi, Critical investigation on the influence of welding heat input and welding residual stress on stress intensity factor and fatigue crack propagation, *Eng. Fail. Anal.* 89(2018) 200-221.

- [37] R. Gadallah, N. Osawa, S. Tanaka, S. Tsutsumi, A novel approach to evaluate mixed-mode SIFs for a through-thickness crack in a welding residual stress field using an effective welding simulation method, *Eng. Fract. Mech.* 197(2018) 48-65.
- [38] Ž. Božić, S. Schmauder, M. Mlikota, M. Hummel, Multiscale fatigue crack growth modelling for welded stiffened panels, *Fatig. Fract. Eng. Mater. Struct.* 37(2014) 1043-1054.
- [39] Ž. Božić, S. Schmauder, H. Wolf, The effect of residual stresses on fatigue crack propagation in welded stiffened panels, *Eng. Fail. Anal.* 84(2018) 346-357.
- [40] T. Xia, P. Yang, C. Li, K. Hu, Numerical research on residual ultimate strength of ship hull plates under uniaxial cyclic loads, *Ocean Eng.* 172(2019) 385-395.
- [41] D. Yanagihara, Y. Miyake, Compressive collapse behavior of stiffened plate with cracking damage, *Proc. Jpn. Soc. Naval Arch. Ocean Eng.* 11(2010) 99-102. (in Japanese)
- [42] D. Yanagihara, Bending and compressive strength of stiffened panels with crack damage in longitudinal stiffeners, *Proc. 24th Int. Offshore and Polar Eng. Conf.* (2014) 671-678.
- [43] C.D. Mote Jr., Global-Local finite element, *Int. J. Numer. Meth. Eng.* 3(1971) 565-574.
- [44] I. Hirai, B.P. Wang, W.D. Pilkey, An efficient zooming method for finite element analysis, *Int. J. Numer. Meth. Eng.* 20(1984) 1671-1683.
- [45] S. Nakasumi, K. Suzuki, H. Ohtsubo, D. Fujii, Mixed analysis of shell and solid elements using overlaying mesh method, *J. Jpn. Soc. Naval Arch. Ocean Eng.* 189(2001) 219-224. (in Japanese)
- [46] S. Tanaka, H. Okada, Y. Watanabe, T. Wakatsuki, Applications of s-FEM to the problems of composite materials with initial strain-like terms, *Int. J. Multiscale Comput. Eng.* 4(2006) 411-428.
- [47] T. Ooya, S. Tanaka, H. Okada, On the linear dependencies of interpolation functions in s-version finite element method, *Jpn. Comput. Sci. Tech.* 3(2009) 124-135.

- [48] N. Osawa, K. Hashimoto, J. Sawamura, T. Nakai, S. Suzuki, Study on shell-solid coupling FE analysis for fatigue assessment of ship structure, *Mar. Struct.* 20(2007) 143-163.
- [49] S. Tanaka, S. Okazawa, H. Okada, Y. Xi, Y. Ohtsuki, Analysis of three-dimensional surface crack in welded joint structure using shell-solid mixed method, *Int. J. Offshore Polar Eng.* 23(2013) 224-231.
- [50] Y. Setoyama, S. Tanaka, D. Yanagihara, C. Murakami, Finite element modeling and ultimate strength evaluation for cracked plates, *Trans. Jpn. Soc. Comput. Eng. Sci.* (2017) 20170014 (in Japanese).
- [51] LS-DYNA, Keyword user's manual Volume I-III, (2015).
- [52] MD Nastran, Quick reference guide, (2006).
- [53] ABAQUS, Keywords reference manual, Version 6.5, (2005).
- [54] ANSYS, Help reference, Version 12.0, (2011).
- [55] H. Matsuda, Buckling/Ultimate strength evaluations for cracked plate structures, Master dissertation, Graduate School of Engineering, Hiroshima University (2016) (in Japanese)